Ferromagnetic resonance spectra in a weak stripe domain structure

N. Vukadinovic,[1] M. Labrune,[2] J. Ben Youssef,[3] A. Marty,[4] J. C. Toussaint,[5] and H. Le Gall[3]
[1]*Dassault Aviation, 92552 Saint-Cloud, France*
[2]*Laboratoire PMTM, Institut Galilée, Université Paris-13, 93430 Villetaneuse, France*
[3]*Laboratoire de Magnétisme de Bretagne, UPRES-A/CNRS, 29285 Brest, France*
[4]*CEA-Grenoble, Département de Recherche Fondamentale sur la Matière Condensée/SP2M, 38054 Grenoble cédex 9, France*
[5]*Laboratoire Louis Néel, CNRS, 38042 Grenoble cédex 9, France*
(Received 29 June 2001; revised manuscript received 5 October 2001; published 27 December 2001)

The ferromagnetic resonance (FMR) spectra in magnetic films with a nonuniform magnetization configuration are known to exhibit multiple absorption peaks. In this paper, the case of ferromagnetic films supporting a weak stripe domain structure is addressed. A two-dimensional dynamic micromagnetic model is used to investigate the high-frequency response of such a magnetic structure. In a first step, the zero-field susceptibility spectra are computed. The existence of numerous resonances resulting from the excitation of surface and volume modes is predicted. The main features of spectra (number of resonances, resonance frequencies, intensities, and linewidths) strongly depend on the equilibrium spin configuration and on the rf exciting field orientation. In a second step, the susceptibility spectra in the presence of an in-plane static magnetic field applied along the stripe direction are studied in detail. The dispersion relation, frequency versus in-plane magnetic field, is computed for each magnetic excitation. These dispersion curves reveal possible mode couplings and interchange of mode characters with increasing magnetic field. The theoretical in-plane FMR spectra are then deduced from the frequency and magnetic field dependence of the dynamic susceptibility. These theoretical results are discussed in light of available experimental FMR data obtained on thin ferromagnetic films with a moderate perpendicular anisotropy.

DOI: 10.1103/PhysRevB.65.054403 PACS number(s): 76.50.+g, 75.60.Ch, 75.70.−i

I. INTRODUCTION

Ferromagnetic resonance (FMR) is one of the most powerful techniques for investigating magnetic thin films.[1,2] In the standard FMR experiment, the derivative of the rf power absorbed by the sample is measured as a function of the applied dc magnetic field at constant microwave frequency (field-swept configuration). In such a procedure, the operating microwave frequency is chosen so that the resonance field associated with the uniform precession mode exceeds the saturation field (saturated state). Magnetic parameters such as the anisotropy constants and gyromagnetic ratio can be determined from the angular dependence of the resonance field.[3] In addition, quantitative information on the relaxation mechanisms of the magnetization can be deduced from the measurement of the FMR linewidth,[4] giving access, for instance, to the Gilbert damping parameter.[5] The determination of previous magnetic parameters is performed by using the Smit-Beljers energy method[6] for which an appropriate form of the magnetic free energy density of the sample in the single-domain state is required. Relatively little attention has been paid to the FMR in the unsaturated state. The major reason arises from an interpretation of FMR spectra which is generally more complex and needs a precise knowledge of the equilibrium magnetic configuration inside the sample. Pioneer works[6–8] were devoted to the FMR in the presence of a simple-domain structure such as lamellar domains. In particular, the case of ferromagnetic garnet films with a large uniaxial perpendicular anisotropy [$Q>1$, where Q is the so-called quality factor defined as $Q=K_U/(2\pi M_s^2)$, with K_U the uniaxial anisotropy constant and M_S the saturation magnetization] supporting parallel stripe domains with alternatively up-and-down magnetization was treated in detail.[9–12] Two domain mode resonances corresponding to precession modes inside the domains with two types of phase relations between neighboring domains and one Bloch domain wall resonance were observed. This multidomain state was theoretically described by assuming the existence of large uniformly magnetized domains separated by infinitely thin one-dimensional (1D) Bloch domain walls (limit of a large Q value). The extended Smit-Beljers formalism including the free energy density of this multidomain state accounts for these magnetic excitations.[10,11] In addition, in such a magnetic system high-order domain wall resonances have been detected and successfully interpreted in terms of flexural domain wall modes.[13–15]

Recently, complicated FMR spectra in the unsaturated state with a series of resonances were reported in Co (Ref. 16) and FePd (Ref. 17) thin films. These films possess a perpendicular anisotropy, but a moderate Q factor ($Q\sim 0.3-0.5$), and present a weak stripe domain structure[18] above a critical thickness. The micromagnetic calculations [3D (Ref. 16) and 2D (Ref. 19)] of the static magnetization configuration exhibit 2D domain walls (Bloch like at the film center and Néel like at the film surfaces) whose thickness represents a significant ratio with respect to the domain width. In addition, the spin orientation inside the domains depends on the film thickness. This nonuniform spin configuration departs from the ideal stripe domain structure considered in the Smit-Beljers model. In consequence, this analytical model cannot reproduce all the features of FMR spectra experimentally observed.

An alternative promising approach consists in using a dynamic micromagnetic simulation.[19,20] High-frequency sus-

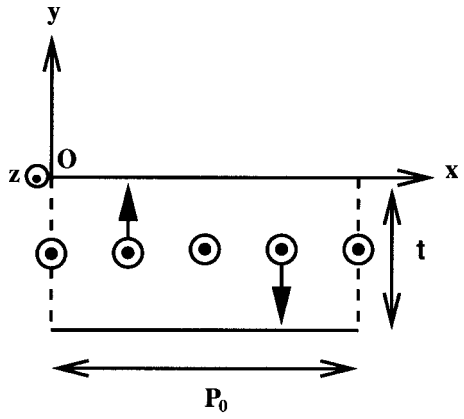

FIG. 1. Cross-sectional schematic representation of the weak stripe domain structure over one period of the pattern and coordinate system. In the 2D micromagnetic simulations, the magnetization is assumed invariant along the *z* axis which coincides with the stripe direction.

ceptibility spectra of ferromagnetic films with a weak stripe domain structure computed by a 2D dynamic micromagnetic model were recently published.[19] These calculations predict the existence of multiple resonances associated with surface and volume modes of stripe domains and were compared successfully with experimental zero-field microwave permeability spectra.

The aim of the present paper is to compute whole FMR spectra in the unsaturated state in terms of mode positions, intensities, and linewidths by using this 2D dynamic micromagnetic model. Ferromagnetic films with a weak stripe domain structure are considered.

This paper is organized as follows: Section II describes the dynamic micromagnetic model. This is followed by a presentation of theoretical zero-field susceptibility spectra exhibiting multiple resonances. The origin of these resonances is correlated with the equilibrium magnetization distribution. The effect of an in-plane dc magnetic field applied along the stripe direction on each magnetic excitation is then investigated in detail. Their dispersion curves, frequency versus in-plane field, are reported. The influence of the uniaxial anisotropy and exchange strength on the dispersion curves is also pointed out. Finally, the theoretical FMR spectra are computed from the frequency and field dependence of the dynamic susceptibility and compared with available experimental FMR data in Sec. III.

II. TWO-DIMENSIONAL DYNAMIC MICROMAGNETIC MODEL OF STRIPE DOMAINS

A. Derivation of the dynamic susceptibility

The dynamic of stripe domains is considered from the micromagnetic point of view, where the magnetic medium is represented as a macroscopic continuum characterized by the magnetization vector $\mathbf{M}(\mathbf{r},t)$ of constant modulus M_S $[\mathbf{M}(\mathbf{r},t)=M_S\mathbf{m}(\mathbf{r},t)]$.[21,22] Let us consider a periodic domain pattern of period P_0; the *x* axis corresponds to the periodicity direction, the *y* axis is the film normal, and the *z* axis is oriented along the stripe direction (Fig. 1). In the 2D micromagnetic simulations, the reduced magnetization $\mathbf{m}$ is assumed invariant along the *z* axis ($\mathbf{r}$ is restricted to vary in the *x*-*y* plane).

The dynamic micromagnetic simulations are performed in two steps.

First, the equilibrium magnetization configuration is computed using a Labonte-Brown-type procedure.[23,24] A relaxation method is used iteratively in order to achieve the alignment of the magnetization vector along the effective field vector at each point of the discretization lattice in the cross section through the periodic cell (*x*-*y*) plane. The effective field incorporates the contributions from exchange, anisotropy, demagnetizing, and dc applied fields, $\mathbf{H}_{\text{eff}}=\mathbf{H}_{\text{exch}}+\mathbf{H}_{\text{anis}}+\mathbf{H}_{\text{demag}}+\mathbf{H}_{\text{app}}$. The explicit forms for each field are given below by adopting the cgs system of units.

The exchange field $\mathbf{H}_{\text{exch}}$ is expressed by

$$\mathbf{H}_{\text{exch}}=\frac{2A}{M_S}\Delta\mathbf{m}, \tag{1}$$

with *A* the exchange constant.

For a first-order uniaxial anisotropy along the *y* axis (unit vector $\mathbf{u}$), the anisotropy field has the following form:

$$\mathbf{H}_{\text{anis}}=\frac{2K_U}{M_S}[(\mathbf{m}\cdot\mathbf{u})\mathbf{u}-\mathbf{m}] \quad (K_U>0). \tag{2}$$

Finally, the nonlocal demagnetizing field is given by:

$$\text{div}\,\mathbf{H}_{\text{demag}}=-\text{div}\,\mathbf{M},$$

$$\text{curl}\mathbf{H}_{\text{demag}}=0. \tag{3}$$

In addition, the boundary conditions are of the Neumann type at the film surfaces (the normal derivative of the magnetization distribution at the surfaces is zero) and are periodic along the *x* axis.

This computation provides the equilibrium magnetization configuration $\mathbf{m}_{\text{eq}}(\mathbf{r})$, the equilibrium field $\mathbf{H}_{\text{eq}}(\mathbf{r})=\mathbf{H}_{\text{eff}}[\mathbf{m}_{\text{eq}}(\mathbf{r})]$, and the stable domain period P_0.

Second, the dynamic susceptibility is determined by computing the response $\delta\mathbf{m}(\mathbf{r},t)$ of the magnetization configuration to a weak uniform magnetic excitation $\delta\mathbf{h}(t)$. The developed code for treating this problem is based on a method recently published[20] and is extended in order to take into account the periodic nature of the magnetization configuration. The time evolution of the magnetic configuration can be described by the Landau-Lifshitz-Gilbert (LLG) equation[5]

$$\frac{d\mathbf{m}}{dt}=-|\gamma|\mathbf{m}\times\mathbf{H}+\alpha\mathbf{m}\times\frac{d\mathbf{m}}{dt}, \tag{4}$$

where $\mathbf{m}$ can be expanded in the form $\mathbf{m}(\mathbf{r},t)=\mathbf{m}_{\text{eq}}(\mathbf{r})+\delta\mathbf{m}(\mathbf{r},t)$, $\mathbf{H}$ represents the total magnetic field that can be written $\mathbf{H}(\mathbf{r},t)=\mathbf{H}_{\text{eq}}(\mathbf{r})+\delta\mathbf{h}(t)+\mathbf{H}_{\text{eff}}(\delta\mathbf{m})$, γ is the gyromagnetic ratio, and α is the Gilbert damping parameter. By considering a harmonic time dependence for $\delta\mathbf{h}$ and $\delta\mathbf{m}$ ($e^{i\omega t}$, ω is the angular frequency) and under the assumptions $|\delta\mathbf{h}|\ll|\mathbf{H}_{\text{eq}}(\mathbf{r})|$, $|\mathbf{H}_{\text{eff}}(\delta\mathbf{m})|\ll|\mathbf{H}_{\text{eq}}(\mathbf{r})|$, and $|\delta\mathbf{m}|\ll|\mathbf{m}_{\text{eq}}|=1$, linearizing of Eq. (4) leads to the following linear system:

$$\left(-\frac{i\omega}{|\gamma|} I + D_2 - D_1 D_H \right) \delta\mathbf{m} = D_1 \delta\mathbf{h}, \tag{5}$$

where I is the unit matrix and the matrices D_1, D_2, and D_H are defined, for any given vector $\mathbf{v}$, by

$$D_1\mathbf{v} = \mathbf{m}_{\mathrm{eq}} \times \mathbf{v},$$

$$D_2\mathbf{v} = \left(\mathbf{H}_{\mathrm{eq}} + \frac{i\alpha\omega}{|\gamma|} \mathbf{m}_{\mathrm{eq}} \right) \times \mathbf{v},$$

$$D_H\mathbf{v} = (\mathbf{H}_{\mathrm{eff}} - \mathbf{H}_{\mathrm{app}})(\mathbf{v}). \tag{6}$$

For a grid with N discretization points, $\delta\mathbf{m}$ and $\delta\mathbf{h}$ are $3N$ vectors and the linear dense system (5) is of size $3N \times 3N$. This system is solved for each frequency by using a direct method (Gauss factorization). The scalar dynamic susceptibility is then given by

$$\chi = \frac{1}{N} \sum_{i=1}^{N} \frac{\delta\mathbf{m}_i \cdot \delta\mathbf{h}_i}{|\delta\mathbf{h}_i|^2}. \tag{7}$$

The computations were performed on a parallel computer with the treatment of one frequency per processor. Different discretization grids were considered. As a conclusion, using a 64×31 grid leads to reliable results for both the static and dynamic micromagnetic computations. The susceptibility spectra presented in the next section were computed over the frequency range from 100 MHz to 30 GHz with a frequency step $\Delta f = 100$ MHz. A refinement ($\Delta f = 10$ MHz) was then performed around the detected resonance frequencies.

Comparisons between this dynamic matrix technique and the direct integration of the LLG equation will be published in a forthcoming article.[25]

B. Zero-field dynamic susceptibility spectra

The zero-field micromagnetic state of thin films with a uniaxial perpendicular anisotropy may be represented in a phase diagram depending on the two reduced parameters: the quality factor Q and, for instance, the ratio of the film thickness t to the exchange length $\Lambda = (A/2\pi M_S^2)^{1/2}$. The reduced critical thickness for domain nucleation was computed using the procedure described in Ref. 18 and is displayed in the $(Q, t/\Lambda)$ plane in Fig. 2. In this phase diagram, a point located above the critical line was selected: point P $(Q = 0.35,\ t/\Lambda = 15.7)$. The magnetic parameters correspond to $4\pi M_S = 13\,190$ G, $K_U = 2.4 \times 10^6$ erg/cm^3, $A = 0.7 \times 10^{-6}$ erg/cm, and $t = 50$ nm and are representative of FePd films with a moderate perpendicular anisotropy supporting a weak stripe domain structure.[26,27] Figure 3(a) exhibits the static magnetization configuration within one period for point P. The arrows represent the components of $\mathbf{M}$ in the plane (Ox,Oy) of the figure. A code color is adopted for imaging the z component. This configuration consists of an open flux pattern with large domains magnetized along the y direction separated by a Bloch wall at the film center surrounded by Néel caps at the film surfaces. The zero-field stripe period corresponds to $P_0 = 109$ nm. The spectra of the scalar dynamic susceptibility (imaginary part χ'') for the three main exciting directions δh_{rf} applied along the x axis (x configuration), y axis (y configuration), and z axis (z configuration) are displayed in Fig. 3(b). The computations were performed using the magnetic parameters $\gamma = 1.85 \times 10^7$ Oe^{-1} s^{-1} and $\alpha = 0.02$. As previously reported,[19] the spectra reveal the existence of multiple resonances whose numbers and positions depend on the direction of δh_{rf}. For the x configuration, the spectrum consists of one intensive peak labeled (1) and a subsidiary one labeled (2) of weak intensity and located at a higher frequency. These resonances are also observed with one order of magnitude weaker at the same frequencies for the y configuration. In addition, a third resonance labeled (3) clearly appears followed by two very weak excitations at higher frequencies. For the z configuration, the spectrum exhibits two large resonances labeled, respectively, (4) and (6). Three weak excitations are also visible. The weak resonance noted, (5), appearing at the lowest frequency is considered because its behavior in the presence of an applied dc magnetic field will be investigated (see Sec. II C). One can remark that the resonance frequencies of different magnetic excitations do not coincide for the y and z configurations. In order to analyze the physical origin of the magnetic excitations of stripe domains, the modulus of $\delta\mathbf{m}$ within one period is reported in Fig. 3(c) for the main resonances (1), (2), (3), (4), (5), and (6). At each resonance frequency, this modulus is normalized by its maximal value. The high levels of $|\delta\mathbf{m}|$ are represented in red, while the low levels are in blue. For mode (1), the maximum values of $|\delta\mathbf{m}|$ appear at surfaces of domains $[x = \pm(k+1/2)P_0/2,\ k = 0,1, \ldots]$ and to a lesser degree within Bloch-type domain walls. In fact, their respective contributions depend mainly on the quality factor Q. As Q increases, the contribution of Bloch domain walls predominates the surface one (see point A in Ref. 19). In addition, the level of $|\delta\mathbf{m}|$ inside the domains represents approximately a quarter of the maximum value of $|\delta\mathbf{m}|$. Due to the large area of domains, their contributions to the dynamic susceptibility are significative. For mode (2), the higher values of $|\delta\mathbf{m}|$ are located at surfaces of domains $[x = \pm(k+1/2)P_0/2,\ k = 0,1,...]$ and within Bloch-type domain walls. Mode (3) is essentially a surface mode.

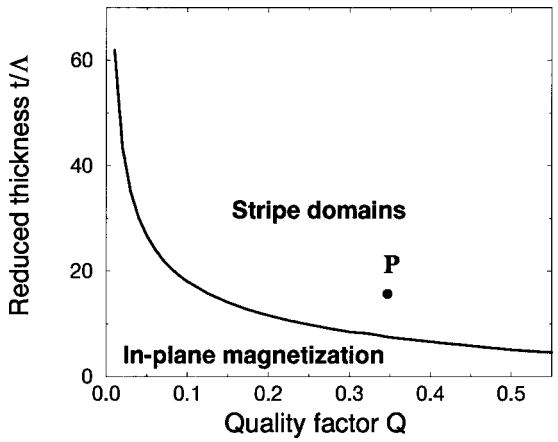

FIG. 2. Phase diagram in the $(Q, t/\Lambda)$ plane. The boundary line represents the reduced zero-field critical thickness t_c/Λ for domain nucleation. Coordinates are (0.35,15.7) for point P.

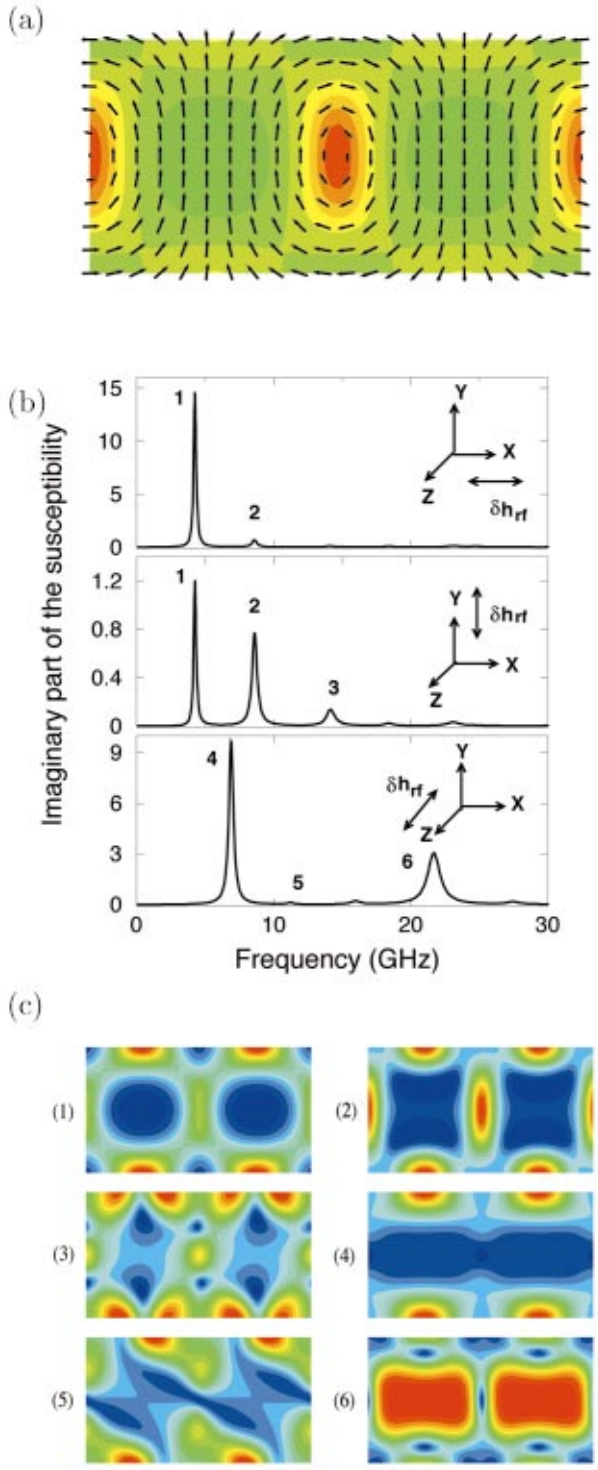

FIG. 3. (Color) (a) Cross-sectional equilibrium magnetization distribution over one period of the pattern corresponding to point *P*. The arrows represent the components of **M** in the plane (*Ox*,*Oy*) of the figure which is perpendicular to the direction (*Oz*) of elongation of the stripe domains. A color code is adopted for imaging the longitudinal (or *z*) component (high levels in red and low levels in green). (b) Corresponding dynamic susceptibility spectra for the three pumping configurations: *x*, *y*, and *z*. (c) $|\delta\mathbf{m}|$ for modes (1), (2), (3), (4), (5), and (6) (high levels in red and low levels in blue).

The maximum values of $|\delta\mathbf{m}|$ occur for $x=\pm(k+1/2)\ P_0/4$, $k=0,1,\ldots$. This mode resembles a spin-wave mode quantized across the domain width [$|\delta\mathbf{m}|\sim|\sin(4\pi/P_0)x|$]. It must be mentioned that for the modes (1), (2), and (3) the spatial variations of $|\delta\mathbf{m}|$ are identical in the *x* and *y* configurations but their magnitudes differ. Mode (4) is a surface mode. The higher values of $|\delta\mathbf{m}|$ are located at surfaces of domains [$x=\pm(k+1/2)P_0/2,\ k=0,1,\ldots$]. Mode (5) appears as a surface mode with an asymmetrical variation of $|\delta\mathbf{m}|$ between the upper and lower interfaces. This mode could correspond to the ''cap shearing mode'' predicted from physical considerations in Ref. 16. Such a mode is characterized by an in-phase motion of all the top caps (top Néel walls) in a given direction ($-x$ in our case) and an in-phase displacement in the opposite direction ($+x$) for all the bottom caps. Mode (6) is a volume mode with the maximum values of $|\delta\mathbf{m}|$ at the center of the domains. In these regions, the spins at equilibrium are essentially oriented along the *y* axis [Fig. 3(a)] and are strongly coupled with δh_{rf} (*z* configuration). The analysis of the in-plane components δm_x and δm_z in neighboring domains indicates that the modes (1), (2), and (3) are acoustic modes (δm_x components in phase between adjacent domains) and the modes (4), (5), and (6) are optic modes (δm_x components out of phase between adjacent domains).

It must be underlined that the zero-field spectra of dynamic susceptibility depend strongly on the location of the sample in the phase diagram as reported in Ref. 19. For a low-*Q* sample (see point *B* in Ref. 19), complicated dynamic susceptibility spectra including an extended frequency response and the existence of a fine structure, mainly observed for the *y* and *z* configurations, are obtained. The strong nonuniformity of static and dynamic effective fields is responsible for such dynamic susceptibility spectra. In contrast, a higher-*Q* sample (see point *A* in Ref. 19) exhibits dynamic susceptibility spectra with well-located resonances. A first study of the influence of the quality factor *Q* (by varying K_U) and the reduced thickness t/Λ (by varying *t*) on the features of susceptibility spectra allows us to point out some rules: (i) the resonance frequencies of the main modes increase with increasing *Q* (at constant t/Λ); (ii) the predominant susceptibility response obtained for the *x* configuration (case of a low-*Q* sample) transforms into responses of equivalent levels for the three configurations as *Q* increases (at constant t/Λ); (iii) as *Q* increases (at constant t/Λ), the number of peaks of the fine structure diminishes and, finally, the fine structure disappears; (iv) for a given low-*Q* factor, the number of peaks of the fine structure increases with increasing thickness while their linewidths decrease. A more systematic study is necessary to generalize these tendencies.

C. In-plane field dependence of dynamic susceptibility spectra

In this section, the effect of an in-plane magnetic field applied along the stripe direction, H_z, on the different magnetic excitations is investigated.

Figure 4 displays the calculated evolutions of the stripe period P_0 and of the *z* component of the static magnetization averaged over the periodic cell $\langle m_z\rangle$ as functions of H_z. As the field value increases, P_0 decreases. Such a profile was

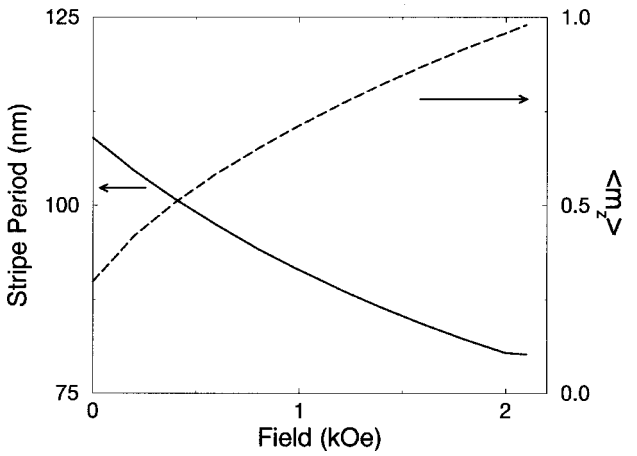

FIG. 4. In-plane field dependences of the stripe period P_0 (solid line) and of the z component of the static magnetization averaged over the whole periodic cell $\langle m_z \rangle$ (dashed line). The in-plane dc magnetic field H_z is applied along the stripe direction. The magnetic parameters correspond to those of point P.

measured using soft x-ray resonant magnetic scattering for FePd films with an intermediate-Q factor.[28] As expected, $\langle m_z \rangle$ increases with H_z. The saturated state $\langle m_z \rangle = 1$ is reached for the field value $H_{\mathrm{sat}} = 2.2$ kOe. The imaginary part of the susceptibility χ'' in the (field, frequency) plane is reported in Fig. 5 for the three configurations of interest [x configuration in Fig. 5(a), y configuration in Fig. 5(b), and z configuration in Fig. 5(c)]. For the x configuration, increasing field produces a shift of the main resonance (1) towards the high frequencies and a decrease of the peak intensity. The second resonance (2) disappears rapidly with increasing field. For the y configuration, the intensity of the resonance (1) is approximately constant as a function of the applied field. The resonances (2) and (3) visible at low and intermediate fields are strongly attenuated as the field increases. For both x and y configurations, only the resonance (1) subsists above the in-plane saturation field and it corresponds to the classical in-plane FMR. For the z configuration, the dynamic response is more complex. The frequencies of the resonances (4) and (6) do not vary monotonously with increasing field. In addition, their intensities decrease with increasing field. On the other hand, the behavior of the resonance (5) is not trivial. This excitation is very weak at low fields: then, its intensity grows and passes through a maximum at intermediate fields before disappearing at higher fields. As expected in the linear regime, no magnetic excitations exist in the saturated state for the z configuration ($\delta h_{\mathrm{rf}} \| H_z$). The dispersion curves, frequency versus in-plane field for each magnetic excitation are reported in Fig. 6 by distinguishing the x and y configurations [Fig. 6(a)] and the z configuration [Fig. 6(b)]. In the former case, the frequencies of the three excitations increase with increasing field. The evolution is linear for resonance (1) except at low fields. For the resonances (2) and (3), their dispersion curves show curvatures, more pronounced for the resonance (2). In the latter case, the frequency of the resonance (4) increases with increasing field, passes through a maximum, and then decreases for higher fields. The frequency of resonance (5) increases monotonously with increasing field. Last, the frequency of the resonance (6) decreases with increasing field, passes through a minimum, and then increases for higher fields. These last features indicate the possible existence of mode coupling. The dispersion curves of the resonances (4), (5), and (6)

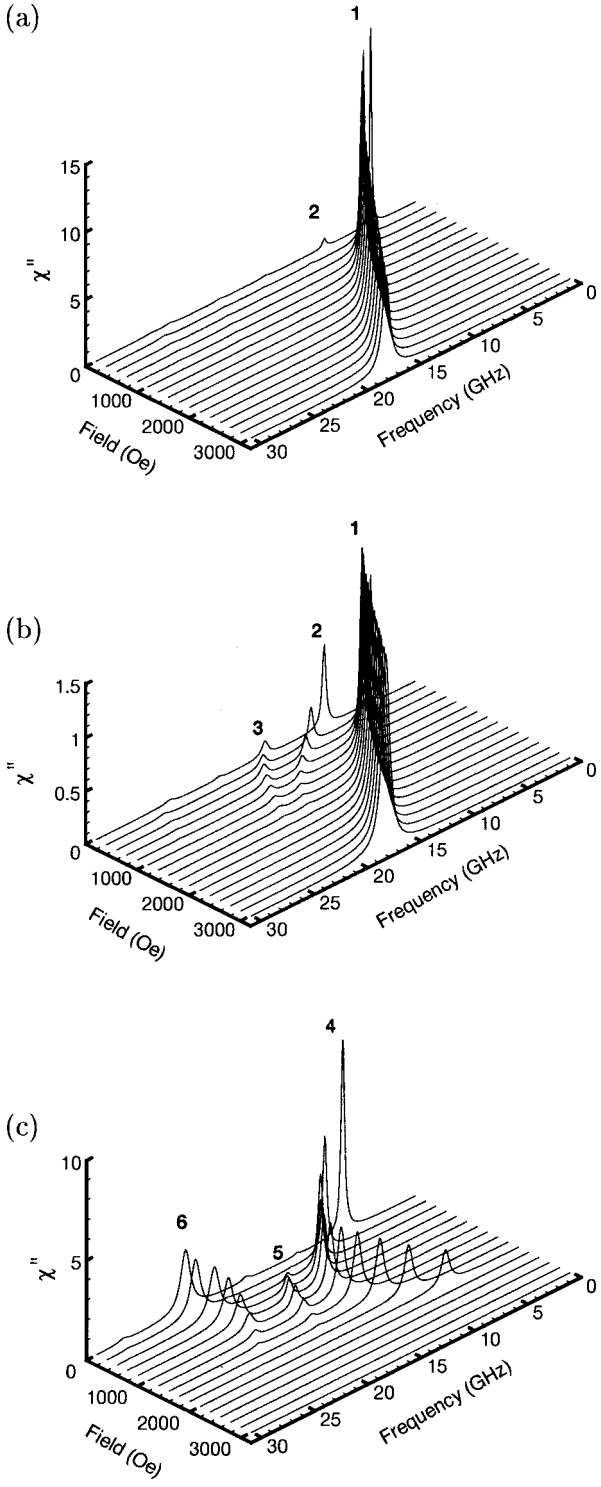

FIG. 5. Imaginary part of the calculated dynamic susceptibility χ'' as a function of the in-plane dc magnetic field H_z and of frequency for point P: (a) x configuration, (b) y configuration, and (c) z configuration. H_z is along the stripe direction.

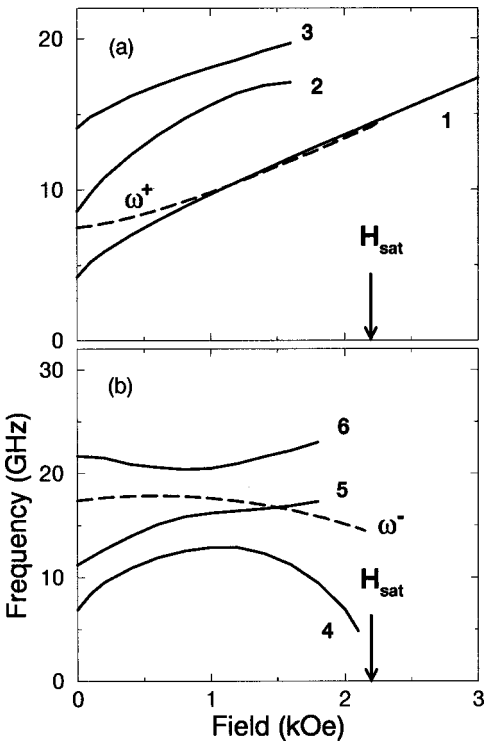

FIG. 6. In-plane dispersion curves, frequency vs applied magnetic field H_z, for the six magnetic excitations computed by the 2D dynamic micromagnetic model (solid lines): (a) x and y configurations and (b) z configuration. The in-plane saturation field H_{sat} is on the order of 2.2 kOe for point P. The in-plane dispersion curves of the two domain modes (acoustic ω^+ and optic ω^-) calculated by the DM-FMR model are also reported (dashed lines).

seem to repel each other in order to avoid the crossing points which gives rise to frequency gaps. Such behaviors were observed in garnet films with a perpendicular anisotropy. In particular, the coupling between the domain wall resonance and the two domain mode resonances in the presence of an in-plane dc magnetic field was analyzed in detail.[10,11] In our case, the existence of three resonance branches makes the dispersion curves more complex. Moreover, it is instructive to compare these dispersion curves with those computed from the domain mode ferromagnetic resonance (DM-FMR) model.[10] It must be borne in mind that this analytical model is based on the assumption of a large Q factor leading to a static magnetization configuration with alternatively up-and-down uniformly magnetized domains (along the y axis). The dispersion curves of the two domain modes predicted by the DM-FMR model and denoted, respectively, ω^+ (acoustic character) and ω^- (optic character) are reported in Fig. 6. Two comments can be made: (i) the resonance frequency of the acoustic mode ω^+ is close to that of mode (1) except at low fields. For $H_z > 1000$ Oe, the DM-FMR model provides a very good approximation of the resonance frequency of mode (1); (ii) the dispersion curve of the optic mode ω^- cannot be associated with any of the dispersion curves computed by the numerical micromagnetic model.

The in-plane field dependence of the main modes (1), (4), (5), and (6) is displayed in Fig. 7. For mode (1), $|\delta\mathbf{m}|$ becomes more and more uniform as H_z increases, and in the vicinity of the in-plane saturation field H_{sat}, $|\delta\mathbf{m}|$ is nearly constant through the sample (in-plane FMR). This behavior explains why the DM-FMR model assuming a uniform acoustic mode is relevant at high fields. A striking feature appearing in Fig. 7 is the change of mode structure as the field increases. Mode (4) corresponding to a surface mode at zero field becomes a volume mode at high fields. Conversely,

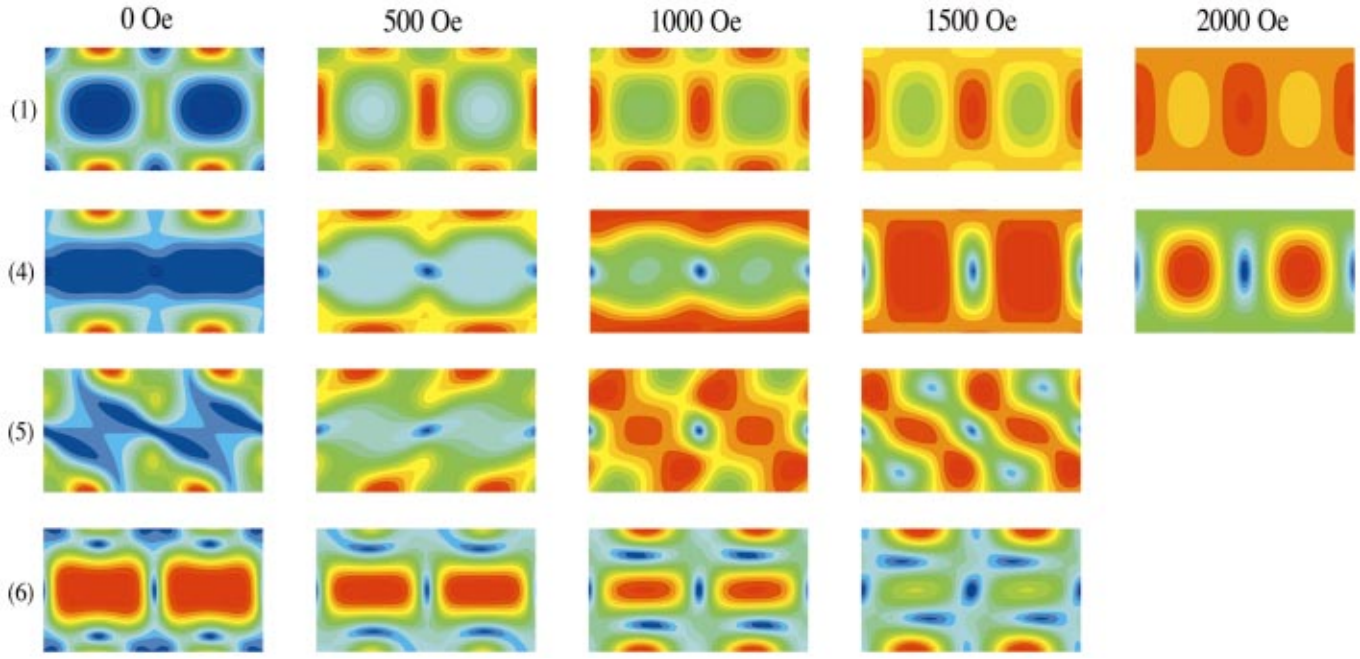

FIG. 7. (Color) In-plane field dependence of the main modes (1), (4), (5), and (6) for point P. The in-plane dc magnetic field H_z is applied along the stripe direction. The color code is the same as in Fig. 3.

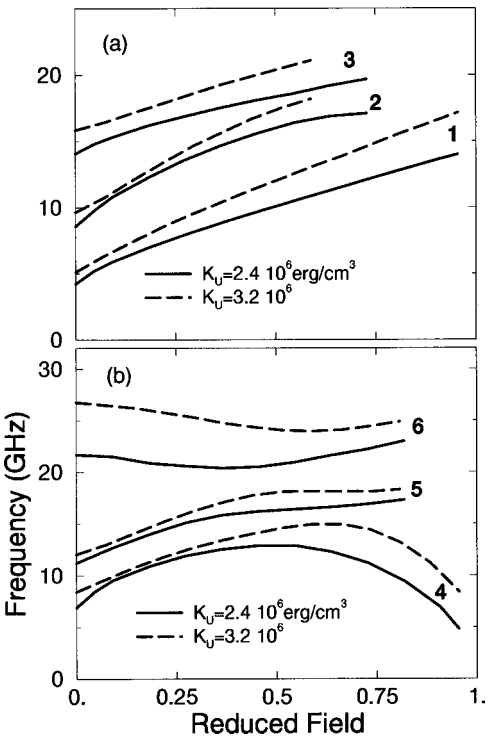

FIG. 8. Effect of the anisotropy constant K_U on the dispersion curves, frequency vs reduced field $H_z/H_{\rm sat}$, for the six magnetic excitations: (a) x and y configurations and (b) z configuration. $K_U=2.4\times10^6$ erg/cm^3 (solid lines) and $K_U=3.2\times10^6$ erg/cm^3 (dashed lines). The other physical parameters are those of point P.

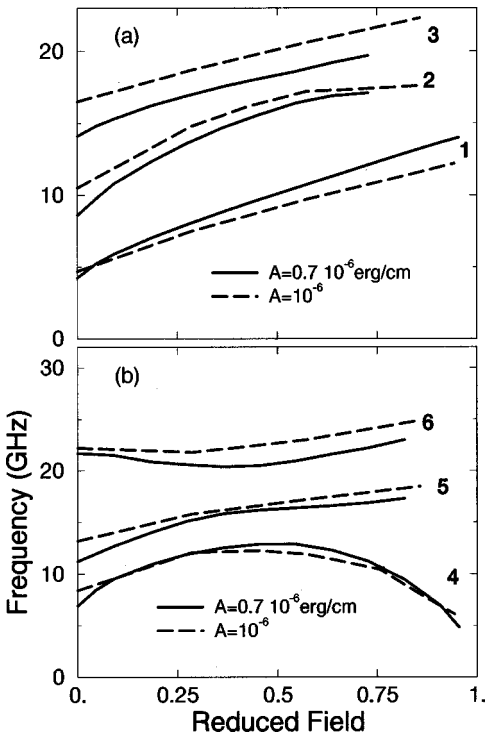

FIG. 9. Effect of the exchange constant A on the dispersion curves, frequency vs reduced field $H_z/H_{\rm sat}$, for the six magnetic excitations: (a) x and y configurations (b) z configuration. $A=0.7\times10^{-6}$ erg/cm (solid lines) and $A=10^{-6}$ erg/cm (dashed lines). The other physical parameters are those of point P.

the volume mode (6) is transformed into a surface mode with increasing field. Such a mode conversion correlates with the existence of mode coupling as observed in the dispersion curves for the z configuration. On passing through the field region of coupling, the structure of modes (4) and (6) is interchanged. A similar phenomenon exists between the two domain mode resonances in garnet films with a perpendicular anisotropy.[11] At low fields, mode (6) is nearly uniform in the core of domains and resembles the uniform optic mode ω^-. For mode (5), asymmetrical variations of $|\delta\mathbf{m}|$ are observed for all the field values. In the field region of coupling, the high values of $|\delta\mathbf{m}|$ are no longer limited to the film surfaces, but extend through the film thickness. In order to investigate the effect of the uniaxial anisotropy on the field dependence of the dynamic susceptibility, micromagnetic computations were performed by replacing $K_U=2.4\times10^6$ erg/cm^3 by $K_U=3.2\times10^6$ erg/cm^3, the other parameters being unchanged. For a given field value, the enhancement of K_U leads to a decrease of $\langle m_z\rangle$ and a slight increase of P_0. The in-plane saturation field corresponds, respectively, to $H_{\rm sat}=2.2$ kOe for $K_U=2.4\times10^6$ erg/cm^3 and $H_{\rm sat}=3.4$ kOe for $K_U=3.2\times10^6$ erg/cm^3. Figure 8 shows the dispersion curves, frequency versus the reduced field $H_z/H_{\rm sat}$, for $K_U=2.4\times10^6$ and 3.2×10^6 erg/cm^3. The increase of K_U induces a shift of the dispersion curves towards higher frequencies for all the resonances. This shift is more important for the resonance (6) and reaches 5 GHz at zero field where this resonance is identified as a nearly homogeneous volume mode. In addition, the curvatures of the dispersion curves for the resonances (1), (2), and (3) are less pronounced for $K_U=3.2\times10^6$ erg/cm^3. In the same manner, the effect of the exchange strength on the field dependence of the dynamic susceptibility was studied. Two values of the exchange strength were considered: $A=0.7\times10^{-6}$ erg/cm and $A=10^{-6}$ erg/cm, the other parameters being unchanged. For a given field value, an enhancement of A leads to an increase of $\langle m_z\rangle$ and a slight increase of P_0. The in-plane saturation field corresponds, respectively, to $H_{\rm sat}=2.2$ kOe for $A=0.7\times10^{-6}$ erg/cm and $H_{\rm sat}=1.75$ kOe for $A=10^{-6}$ erg/cm. Figure 9 displays the dispersion curves computed for $A=0.7\times10^{-6}$ and 10^{-6} erg/cm. For resonance (1), the slope of the dispersion curve is changed by varying the exchange constant. For the resonances (2), (3), (5), and (6), the increase of A leads to a shift of the dispersion curves towards higher frequencies. The resonance (4) is weakly affected by the variation of A.

III. IN-PLANE FMR SPECTRA

The microwave power P_a absorbed by a sample of volume V from the rf magnetic field is defined by[29]

$$P_a=\left(\int_V dV\,\delta\mathbf{h}_{\rm rf}\cdot\frac{d\mathbf{m}}{dt}\right)_{\text{time average}}. \tag{8}$$

Assuming a harmonic time dependence for $\delta\mathbf{h}$ and $\delta\mathbf{m}$ and a uniform exciting field $\delta\mathbf{h}$, the power absorbed per unit vol-

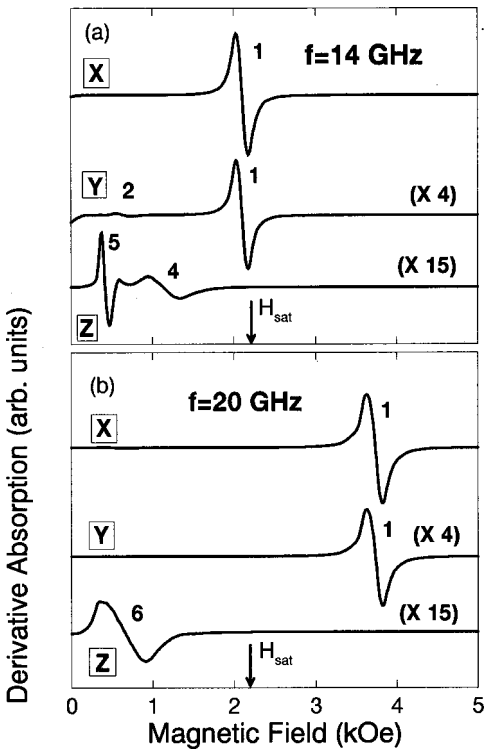

FIG. 10. Theoretical derivative in-plane FMR spectra for the three pumping configurations at 14 GHz (a) and at 20 GHz (b). Case of point *P*.

ume at the frequence f in the presence of the in-plane dc magnetic field H_z takes the following form:

$$P_a(f,H_z)=\pi f\chi''(f,H_z)\,\delta h_{\mathrm{rf}}^2. \tag{9}$$

Knowing the frequency and in-plane field dependences of the susceptibility from dynamic micromagnetic simulations, the theoretical absorbed power can be determined. According to the experimental in-plane FMR spectra, the derivative power absorption dP_a/dH_z is computed as a function of H_z. As an illustrative example, Fig. 10 displays theoretical derivative in-plane FMR spectra at 14 GHz [Fig. 10(a)] and at 20 GHz [Fig. 10(b)] for the configurations *x*, *y*, and *z*. For each frequency, the spectrum is computed with a field step $\Delta H_z=100$ Oe. A refinement ($\Delta H_z=20$ Oe) is performed around the detected resonance lines. At 14 GHz, only the resonance (1) is observed for the *x* configuration. Its resonance field is slightly lower than the in-plane saturation field. For the *y* configuration, the resonance (1) clearly appears. The resonance (2) corresponds to the small oscillation visible around $H_z=600$ Oe. The weak zero-field microwave absorption is due to the resonance (3). At 14 GHz, only the high-field side of this resonance is detected. For the *z* configuration, the two weak signals correspond, respectively, to the resonances (4) and (5). At 20 GHz, the in-plane FMR [resonance (1)] appears for the *x* and *y* configurations. For the *z* configuration, the low-field signal corresponds to the resonance (6). It must be underlined that the observation of the resonances (4) and (6) is due to their respective frequency linewidths, their dispersion curves being not intersected at 14 and 20 GHz, respectively.

These theoretical results can be discussed in light of some available FMR data. First, experimental in-plane FMR spectra were reported on a FePd thin film over the frequency range 6–18 GHz.[17] The FePd thin films were prepared using molecular beam epitaxy under ultra high vacuum (10^{-7} Pa). The growth procedure consists in a deposition of alternate atomic layers of pure Fe and Pd at room temperature.[26] These films possess a directional short range chemical order[30] responsible for a moderate perpendicular magnetic anisotropy (uniaxial type) on a macroscopic scale. The occurrence of a well-organized periodic stripe domain structure above a critical thickness $t_c\sim 30$ nm has been checked by zero-field MFM measurements.[26] The magnetic parameters of the selected sample deduced from vibrating sample magnetometer (VSM) and FMR measurements are quite close to those of point *P* ($4\pi M_S=13\,190$ G, $K_U=2.4\times10^6$ erg/cm^3). The film thickness is $t=50$ nm. The zero-field stripe period P_0 is estimated to be 110 nm from MFM images which is consistent with the computed value $P_0=109$ nm assuming $A=0.7\times10^{-6}$ erg/cm. The gyromagnetic ratio γ is equal to 1.85×10^7 Oe^{-1} s^{-1}. The Gilbert damping parameter determined from the frequency dependence of the perpendicular resonance field associated with the uniform precession mode (saturated state) corresponds to $\alpha=2\times10^{-2}$.

FMR measurements were performed by using a highly sensitive wideband resonance spectrometer with nonresonant microstrip transmission line described elsewhere.[31,32] This alternate technique with respect to the conventional resonant cavity measurements appears more appropriate for investigating the frequency dependence of magnetic resonances.[33] The dc field H_z was applied along the stripe direction.

Figure 11 shows the comparison between the theoretical (no fitting parameters) and experimental in-plane dispersion curves. The field evolution of the experimental low-frequency signal [circles, Fig. 11(a)] coincides with the computed one for the resonance (1). A fairly good agreement is found between the field dependence of the experimental high-frequency signal [triangles, Fig. 11(b)] and the theoretical resonance (4) for $H_z<800$ Oe. At higher fields, the experimental resonance frequency continues to increase, while the micromagnetic computations predict a decrease of the resonance frequency with increasing field. In addition, the apparition of an experimental weak resonance (squares) is not reproduced by the micromagnetic computations. An explanation can be advanced for interpreting these disagreements. It was shown[26] that this FePd film exhibits a standing spin-wave spectrum in which the mode separations approach a linear variation in the mode number. This behavior reflects the existence of a volume inhomogeneity in the internal magnetic properties. A weak thickness dependence of the uniaxial anisotropy induced by the growth procedure seems to be a possible source volume inhomogeneities for this sample. The thickness dependence of K_U could play a major role in the field region of coupling where the transformations between surface and volume modes occur (see Sec. II C) and,

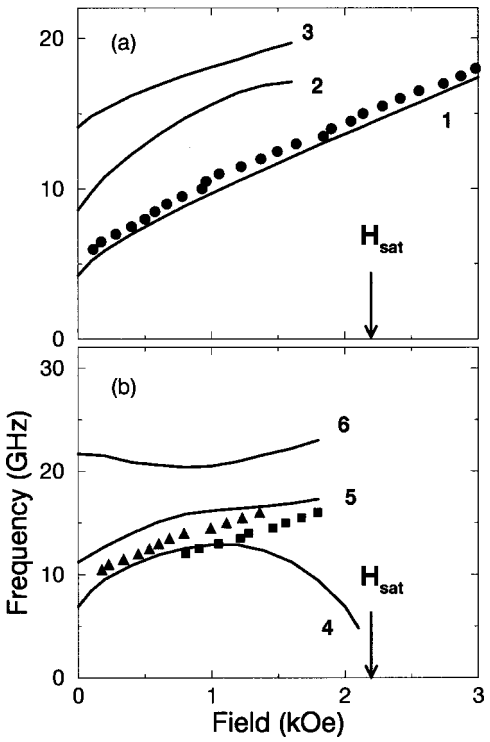

FIG. 11. Theoretical (solid lines) and experimental (points) in-plane dispersion curves: (a) *x* and *y* configurations and (b) *z* configuration. The experimental in-plane FMR data were reported in Ref. 17 and correspond to a FePd thin film whose magnetic parameters are close to those of point *P*.

consequently, could affect the dispersion curves of the modes (4), (5), and (6). Further information on the anisotropy profile across the film thickness and the introduction of such an inhomogeneity into the dynamic micromagnetic simulations seem to be necessary to gain a better understanding.

It is worth noting that these experimental data were previously analyzed by means of the DM-FMR model in Ref. 17. The field dependence of resonance frequencies associated with the two high-intensity signals (circles and triangles in Fig. 11) was fitted with the resonance conditions of the two domain modes. The stripe period P_0 was considered as a free parameter. As a result, the experimental dispersion curves were correctly reproduced by these analytical expressions provided P_0 decreases rapidly as H_z increases $[P_0(H_z=0)/P_0(H_z \rightarrow H_{sat}) \sim 4]$. However, micromagnetic simulations (see Fig. 4) show that P_0 decreases much more slowly with H_z $[P_0(H_z=0)/P_0(H_z \rightarrow H_{sat}) \sim 1.4]$. In fact, the main difficulty, also reported in Ref. 16, arises from the fit of the high-intensity signal for the *z* configuration (triangles in Fig. 11) with the dispersion curve of the mode ω^-, even at low fields. For the *z* configuration, the micromagnetic computations indicate that three main resonances exist and that this experimental line could be identified with the strongly nonuniform mode (4) whose dispersion curve (Fig. 6) largely differs from the one associated with the mode ω^-. Such a disagreement, reveals the limits of the DM-FMR model for describing the dynamic response of magnetic films with a moderate perpendicular anisotropy.

Second, rich in-plane FMR spectra in Co(1111) thin films were also published.[16] In the phase diagram, the coordinates of the selected sample are (0.5,32) for $A=10^{-6}$ erg/cm. The larger value of Q with respect to our point P leads to a shift of the dispersion curves towards higher frequencies. Among the reported multiple magnetic excitations, a resonance [labeled (5) in Ref. 16] is experimentally observed at 22.3 GHz in the low-field region when both the rf and dc fields are parallel to the stripe direction. Based on our computations, this line could be associated with the resonance (6) which is shown in Fig. 11 for the spectrum computed at 20 GHz (*z* configuration).

IV. CONCLUSION

A 2D dynamic micromagnetic code was used for investigating the magnetic excitations of perpendicular anisotropy thin films with a weak stripe domain structure. The theoretical zero-field dynamic susceptibility spectra over the frequency range 0.1–30 GHz reveal numerous resonances whose number and resonance frequencies depend on the direction of the rf exciting field. A modal analysis permitted us to correlate these resonances with spin regions (domains, Bloch and Néel domain walls, etc.) of the stripe domain structure. The evolution of these magnetic excitations in the presence of an in-plane dc magnetic field applied along the stripe direction was studied in detail. The dispersion relation in the (field, frequency) plane was computed and pointed out complex behaviors. In particular, mode couplings might exist between the three resonance branches when both the rf and dc magnetic fields are parallel to the stripe direction. From the field and frequency dependence of the dynamic susceptibility, the theoretical in-plane FMR spectra were determined for the three main pumping configurations. As exemplified, a first analysis of experimental in-plane FMR spectra was performed with the help of the dynamic micromagnetic simulations, making possible the assignment of some magnetic excitations. Further comparisons with experimental FMR data on thin magnetic films with different locations in the phase diagram should be of a great interest. Beyond the case of the weak stripe domain structure, the dynamic micromagnetic simulations offer a path for interpreting complex FMR data in the unsaturated state inaccessible to conventional analytical models.

[1] S. V. Vonsovskii, *Ferromagnetic Resonance* (Pergamon, Oxford, 1966).
[2] M. Farle, Rep. Prog. Phys. **61**, 755 (1998).
[3] H. Makino and Y. Hidaka, Mater. Res. Bull. **16**, 957 (1981).
[4] W. Platow, A. N. Anisimov, G. L. Dunifer, M. Farle, and K. Baberschke, Phys. Rev. B **58**, 5611 (1998).
[5] T. L. Gilbert, Phys. Rev. **100**, 1243 (1955).
[6] J. Smit and H. G. Beljers, Philips Res. Rep. **10**, 113 (1955).
[7] J. O. Artman, Phys. Rev. **105**, 62 (1957).
[8] J. O. Artman, Phys. Rev. **105**, 74 (1957).

[9] J. O. Artman and S. H. Charap, J. Appl. Phys. **49**, 1587 (1978).
[10] M. Ramesh and P. E. Wigen, J. Magn. Magn. Mater. **74**, 123 (1988).
[11] B. Lührmann, H. Dötsch, and S. Süre, Appl. Phys. A: Solids Surf. **57**, 553 (1993).
[12] N. Vukadinovic, J. Ben Youssef, and H. Le Gall, J. Magn. Magn. Mater. **150**, 213 (1995).
[13] J. C. Slonczewski, J. Magn. Magn. Mater. **23**, 305 (1981).
[14] S. Batra and P. E. Wigen, J. Appl. Phys. **61**, 4207 (1987).
[15] N. Vukadinovic, A. Serraj, H. Le Gall, and J. Ben Youssef, Phys. Rev. B **58**, 385 (1998).
[16] U. Ebels, P. E. Wigen, and K. Ounadjela, Europhys. Lett. **46**, 94 (1999).
[17] N. Vukadinovic, H. Le Gall, J. Ben Youssef, V. Gehanno, A. Marty, Y. Samson, and B. Gilles, Eur. Phys. J. B **13**, 445 (2000).
[18] A. Hubert and R. Schaefer, *Magnetic Domains* (Springer, New York, 1998).
[19] N. Vukadinovic, O. Vacus, M. Labrune, O. Acher, and D. Pain, Phys. Rev. Lett. **85**, 2817 (2000).
[20] S. Labbé and P. Y. Bertin, J. Magn. Magn. Mater. **206**, 93 (1999).
[21] W. F. Brown, Jr., *Micromagnetics* (Wiley-Interscience, New York, 1963).
[22] M. E. Schabes, J. Magn. Magn. Mater. **95**, 249 (1991).
[23] A. E. Labonte, J. Appl. Phys. **40**, 2450 (1969).
[24] M. Labrune and J. Miltat, IEEE Trans. Magn. **MAG-26**, 1521 (1990).
[25] A. Marty, J. C. Toussaint, and N. Vukadinovic (unpublished).
[26] V. Gehanno, R. Hoffmann, Y. Samson, A. Marty, and S. Auffret, Eur. Phys. J. B **10**, 457 (1999).
[27] J. Ben Youssef, H. Le Gall, N. Vukadinovic, V. Gehanno, A. Marty, Y. Samson, and B. Gilles, J. Magn. Magn. Mater. **202**, 277 (1999).
[28] A. Marty, Y. Samson, B. Gilles, M. Belakhovsky, E. Dudzik, H. Dürr, S. S. Dhesi, and G. van der Laan, J. B. Goedkoop, J. Appl. Phys. **87**, 5472 (2000).
[29] M. Sparks, *Ferromagnetic Relaxation Theory* (McGraw-Hill, New York, 1964).
[30] V. Gehanno, C. Revenant-Brizard, A. Marty, and B. Gilles, J. Appl. Phys. **84**, 2316 (1998).
[31] E. C. Myers, S-Y. Bi, S. H. Charap, and J. O. Artman, J. Appl. Phys. **53**, 2098 (1982).
[32] H. Le Gall and N. Vukadinovic, IEEE Trans. Magn. **MAG-24**, 3051 (1988).
[33] C. E. Patton, J. Appl. Phys. **39**, 3060 (1968).